In-Situ Simultaneous Small- and Wide-Angle X-ray Scattering Study of Poly(ether ester) during Cold Drawing

A. Nogales,[†] I. Sics,[‡] T. A. Ezquerra,*[,†] Z. Denchev,[§] F. J. Balta Calleja,[†] and B. S. Hsiao[‡]

Instituto de Estructura de la Materia (C.S.I.C.), Serrano 121, Madrid, Spain, Department of Chemistry, State University of New York at Stony Brook, Stony Brook, New York 11794-3400, and University of Minho, Campus Azurem, Guimaraes, Portugal

Received July 11, 2002

ABSTRACT: The cold drawing of a poly(ether ester) block copolymer was studied by in-situ simultaneous small- and wide-angle X-ray scattering techniques in combination with a tensile stretching apparatus. The results obtained revealed three distinct regions in the stress−strain relationship. At low strains ($0 < \epsilon < 18\%$), the applied stress caused extension of the amorphous regions, formed by PTMO and some noncrystallizable segments of PBT, and subsequently reorientation of PBT crystalline lamellae. At slightly higher strains the lamellae become perpendicularly aligned to the drawing direction. At intermediate strains ($18\% < \epsilon < 80\%$), the elongation gradually leads to breakage of the lamellae into smaller pieces, which eventually formed microfibrils containing linear assembly of layered lamellae. At large strains ($\epsilon > 80\%$), a further extension of the PTMO amorphous chains resulted in the fracture of the sample. The pathway of the structural changes by deformation in the present study was slightly different than those observed in the predrawn samples.

Introduction

Thermoplastic elastomers represent a new class of engineering plastics that combine high-temperature mechanical strength and low-temperature flexibility.[1] From the molecular standpoint, these copolymers contain chains of alternating crystalline high melting temperature blocks (hard segments) and noncrystalline blocks (soft segments) with a low glass transition temperature. Segmented poly(ether ester) copolymers belong to the family of such thermoplastic elastomers, which have attracted some special attention recently. These copolymer series consist of hard blocks with multiple ester units such as poly(butylene terephthalate) (PBT) and of soft blocks with multiple ester glycols units such as poly(tetramethylene oxide) (PTMO).[2] In these copolymers, the hard segments are crystallized forming rigid domains, where the soft segments are rubbery with the glass transition temperatures below room temperatures. The microphase domain structure of segregated hard and soft segments is mainly responsible for the mechanical properties of these polymers.[2] The crystalline hard segment domains act as physical cross-links and thus result in the elastomeric character of the material. Copolymer properties can be altered in a wide range by changing the block length of the hard and soft segments.[3]

The elastomeric behavior of these materials is highly dependent on the microphase separation. There have been several studies dealing with the macroscopic mechanical properties of the poly(ether ester) copolymers.[2−4] The behavior of these systems under mechanical deformation is of particular interest because of its practical implications. Tashiro et al. reported that the PBT homopolymer could undergo a solid-state phase transition in the crystalline phase (from α to β form).[5] At high strains, the metastable β form was induced by stress; when the strain was released, the α form was recovered. In other words, the strain-induced phase transition was completely reversible by mechanical deformation. The main difference between the α and β forms was found to be in the conformation state of the methylene sequences in PBT.[5] In block copolymers of PBT and PTMO, a strain-induced phase transition was also observed.[6] The transition in these copolymers, however, did not occur abruptly, as in the PBT homopolymer. The transition was found to take place over a wide range of applied stress, which was attributed to the presence of the soft segment (PTMO) matrix with different volume fractions.[6] Further investigations have been carried out to study the relationships between the macroscopic and microscopic deformation behavior of these block copolymers, mainly by using wide-angle X-ray scattering (WAXS) and small-angle X-ray scattering (SAXS) techniques.[6−8] The initial sample for these studies was always in an oriented state, prepared by drawing and annealing of the specimen under tension.

The aim of the present investigation is to establish direct relationships between the macroscopic deformation behavior and the structure at a microscopic level. Experiments were carried out by simultaneous SAXS/WAXS using synchrotron radiation in combination with a symmetrical tensile stretching machine. The stress−strain curve and the corresponding changes in microstructure were obtained in real time during uniaxial deformation of an initially isotropic block copolymer containing segmented PBT and PTMO moieties.

Experimental Section

Materials. The material studied was a poly(ether ester) segmented block copolymer (trade name ARNITEL EM 550, DSM) consisting of PBT as hard segments and PTMO as soft segments. The weight percentage of the hard segments based on PBT was about 50%. The morphology in this copolymer consisted of semicrystalline PBT domains dispersed in the soft

[†] Instituto de Estructura de la Materia (C.S.I.C.).
[‡] State University of New York at Stony Brook.
[§] University of Minho.

10.1021/ma0210877 CCC: $25.00
Published on Web 06/04/2003

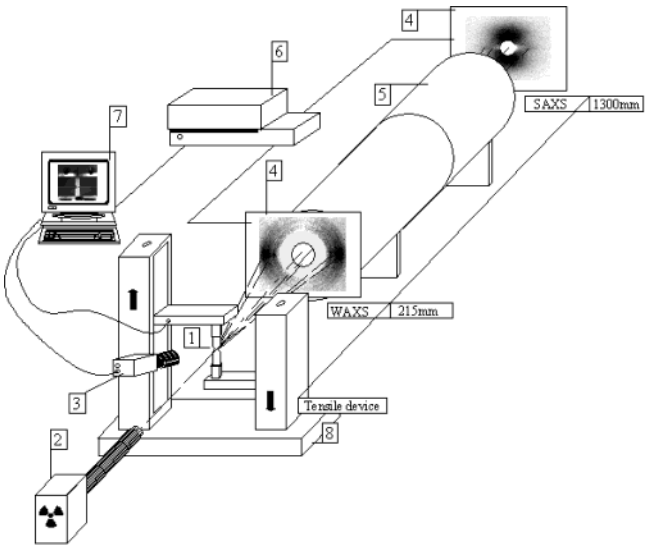

Figure 1. Scheme of the experimental setup: (1) sample, (2) X-ray synchrotron beam, (3) optical CCD camera, (4) WAXS and SAXS image plates, (5) evacuated optical path, (6) image plate scanner, (7) computer and drawing experimental setup, (8) tensile machine.

matrix of amorphous PTMO.[7,8] The average molecular weight of both hard and soft segments was approximately 1500 g/mol each. The overall molecular weight of the copolymer was approximately 25 000 g/mol. The melting temperature of the PBT blocks was 185 °C. The selected poly(ether ester) was extruded at 220 °C. The specimens were prepared by compression-molding the block copolymer at 220 °C into 0.7 mm thick plates. The plates were subsequently cut into rectangular stripes of 60 × 5 mm with two semicircular cutouts of an approximate radius of 3 mm in the middle for mechanical testing. The central cutouts were to ensure that yielding always occurs in the middle of the specimen where the X-ray beam irradiated.

Synchrotron Characterization. In-situ simultaneous SAXS and WAXS measurements were performed on the X3A2 beamline at the National Synchrotron Source (NSLS) at Brookhaven National Laboratory in Upton, NY. The synchrotron radiation was monochromatized to 1.54 Å. Two-dimensional SAXS and WAXS patterns were recorded on two Fuji HR-VTM imaging plates (200 × 250 mm) with sample-to-detector distances of 1300 and 215 mm, respectively. The WAXS imaging plate contained a central opening with a diameter of 20 mm to allow the passage of the SAXS signal (see Figure 1). A FUJI BAS2000 IPTM imaging plate scanning station was used to digitize the image recorded on the plates. The patterns were digitized at a resolution of 100 μm/pixel. The SAXS scattering angle was calibrated by a rat-tail tendon standard; the WAXS scattering angle was calibrated by an Al_2O_3 diffraction standard from the National Institute of Standards and Technology (NIST).

Experimental Procedure. The samples, with an initial length of about 15 mm, were placed in the grips of a model 4442 Instron tensile testing apparatus for measurements. The Instron apparatus was mounted in such a way that the center of the sample was in the beam path, as shown in Figure 1. This machine provided symmetric deformation where the irradiated area remained unchanged in the beam path. After the samples were mounted and placed into the Instron grips, the extension was applied at a crosshead speed of 5 mm/min. Simultaneous SAXS and WAXS images were recorded at collection times of 60 s at selected levels of extension. Because of the small speed used, the error in extension within one collected frame was estimated to be 5 mm. The scattering patterns were corrected for decay of the primary intensity beam over time. SAXS and WAXS patterns of the system without a sample were subtracted from the sample patterns to correct for air and instrumental scattering.

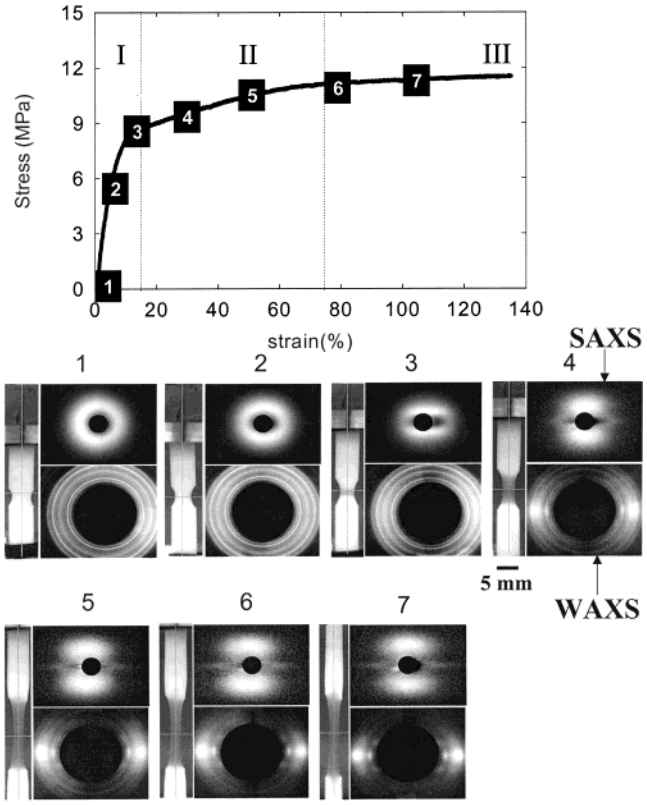

Figure 2. Stress−strain curve for PBT−PTMO copolymer at room temperatures. The panels show, for specific values of strain and stress, the simultaneously collected WAXS (upper) and SAXS (lower) patterns. On the left-hand side of each panel is the corresponding photograph of the sample during drawing.

Results

Figure 2 shows the engineering stress−strain curve for the PBT−PTMO copolymer obtained during drawing. The panels below show in-situ simultaneous WAXS (bottom image) and SAXS (top image) patterns collected at selected strains. On the left-hand side of each X-ray scattering image panel the corresponding photograph of the sample during deformation is shown. The cross hair in the photograph of the stretched sample indicates the exact location where the X-ray beam irradiated. The simultaneously collected WAXS and SAXS patterns show conspicuous changes with increasing applied strain, indicating a profound impact of the mechanical properties onto the microscopic morphology.

The stress−strain curve can be divided into three distinct regions according to the changes in microstructure (dotted lines in Figure 2). At strains lower than 12% (region I), the deformation is elastic, exhibiting a sharp increase in the stress. In this region, the WAXS pattern remains unchanged, showing typical scattering features from the undeformed sample. WAXS patterns in this region consist of circular (Debye) diffraction rings corresponding to Bragg reflections of the α form PBT crystals. The observed diffraction peaks can be assigned as (011) at $2\theta = 16°$, (010) at $2\theta = 17.3°$, (−111) at $2\theta = 20.5°$, (100) at $2\theta = 23.1°$, and (111) at $2\theta = 25°$.[9]

The corresponding SAXS patterns exhibit a different evolution with the increase in strain. The initial SAXS pattern from the undeformed sample consists of an isotropic ring with single scattering maximum, reflecting the separated microphase domains from soft and hard segments. For strains larger than 12%, the broad SAXS ring becomes gradually anisotropic, with the

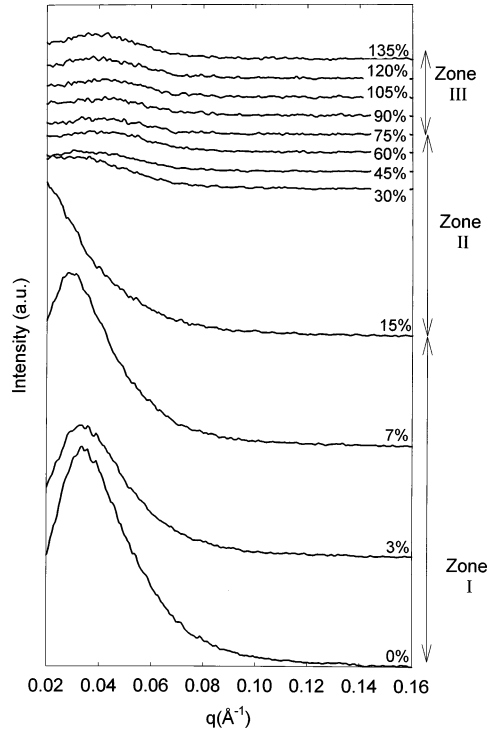

Figure 3. Sliced meridional linear intensity profiles from the SAXS patterns during in-situ deformation. The labels indicate the applied strain in each case. For the sake of clarity, all curves have been vertically shifted.

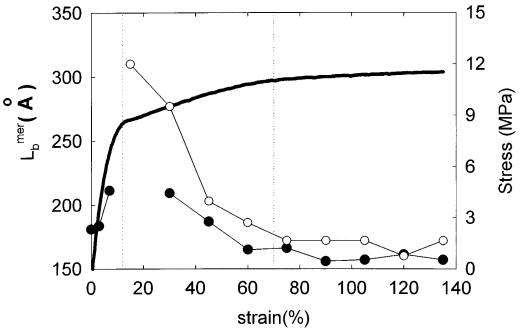

Figure 4. Meridional long spacing as a function of applied stress as calculated by Bragg's law (●). Bragg's law derived spacing obtained from the SAXS projected intensity $I_1(q_3)$ (○).

intensity accumulated along the stretching direction (meridian) increasing with strain. To analyze the positional changes of the SAXS maximum with strain, linear one-dimensional (1D) slices were extracted along the meridional direction of the 2D SAXS patterns. Linear intensity profiles plotted against the scattering vector ($q = 4\pi/\lambda(\sin\theta)$, λ being the wavelength and 2θ the scattering angle) at different strains are illustrated in Figure 3. The position q_m of the meridional maximum is related to the long period $L_b{}^m$ as

$$q_m = 2\pi/L_b{}^m \tag{1}$$

In Figure 3, the initial scattering maximum at $\epsilon = 0\%$ in the meridional intensity profile is located at $q \approx 0.036$ Å^{-1}. At $\epsilon = 15\%$, the peak is seen to shift toward smaller angles and goes out of the range of detection. Figure 4 illustrates the variation of the meridional long spacing $L_b{}^m$ (between the segregated microphase) with the applied strain. To facilitate comparison, the stress−strain curve is superimposed in the same figure. The

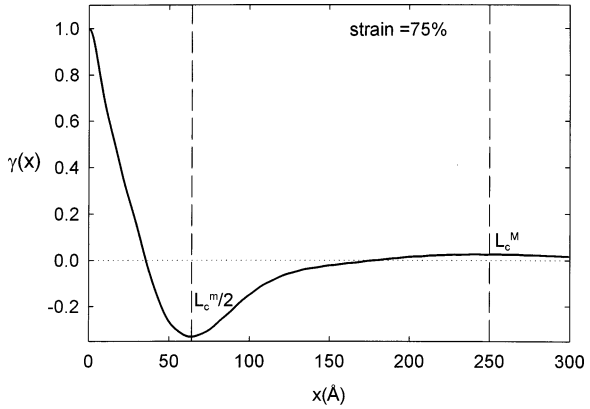

Figure 5. Example of correlation function $\gamma(x)$ obtained from the meridional SAXS projected intensity $I_1(q_3)$. Strain 75%.

initial long spacing increases linearly with strain during the region of elastic deformation (region I: $0\% < \lambda < 12\%$). The maximum measurable long period value of 157 Å is seen at a strain = 7% in Figure 3.

For strains higher than 7%, the SAXS patterns exhibit cylindrical symmetry. In these cases, a projection operation was applied to obtain the integrated intensity on the meridian ($I_1(q_3)$) using the expression

$$I_1(q_3) = \int_0^\infty I(q_{12},q_3) q_{12}\, \mathrm{d}q_{12} \tag{2}$$

Here, the subscript 3 represents the meridional direction. For the sake of comparison, the values of the long spacing obtained according to eq 1 in the projected intensity have been represented in Figure 3 together with the long spacing obtained from a simple meridional cut. The correlation function formalism was applied to this integrated intensity in order to obtain more accurate information on the lamellar structure of the system. To obtain the correlation function, a 1D Fourier transformation was applied to $I_1(q_3)$:

$$\gamma(x) = \frac{\int_0^\infty I_1(q_3)\cos(q_3 x)\, \mathrm{d}q_3}{\int_0^\infty I_1(q_3)\, \mathrm{d}q_3} \tag{3}$$

As an example, the correlation function from the meridional projected intensity $I_1(q_3)$ is shown in Figure 5 for the SAXS pattern corresponding to a strain of 75%. In addition to the long spacing calculated by application of Bragg's law (eq 1), the correlation function formalism provides a tool to obtain additional estimates of the long spacing: (1) from the position of the first maximum ($L_c{}^M$); (2) from twice the position of the first minimum ($L_c{}^m$). From the disparity of all these estimations, one may derive some conclusions on the width of the thickness distribution of the two phases present in the system. As pointed out by Strobl et al. for an ideal 1D two-phase model system, $L_c{}^M = L_c{}^m$.[10] Table 1 shows the values for the long spacing from the projected intensities obtained by the different methods.

In region II ($12\% < \epsilon < 75\%$), the rate of increase of the stress is still positive, but it exhibits a smaller value than that in region I. The stress in region II varies almost linearly with increasing strain. In this region, the corresponding WAXS patterns become oriented, showing features of arcing in all Bragg reflections along the equatorial direction. At the highest strain of this region, a hybrid structure of arcs and multiple spots of

Table 1. Structural Parameters of the Studied Sample during Stretching, As Derived by Various Methods of Analysis

	strain (%)	L_b (Å)	L_b^1 (Å)	L_c^{M1} (Å)	L_c^{m1} (Å)
region I	0	180			
	3	184			
	7	210	321	>300	187
region II	15		310	>300	214
	30	210	277	>300	143
	45	185	203	>300	138
	60	165	186	292	133
	75	168	172	241	128
region III	90	158	172	277	132
	105	160	172	289	126
	120	163	160	249	128
	135	160	172	242	120

reflections around the equator is observed (Figure 2). It is interesting to note that the (011) reflection splits into four symmetric spots aligned along two off-axes with the same inclined angle with respect to the equator, whereas (010) and (100) reflections turns into two sets of distinct equatorial peaks.

The WAXS patterns were azimuthually integrated. The obtained intensities vs scattering angle (2θ) are presented in Figure 6. Values on the right-hand side of the curves denote the applied strains. These curves were deconvoluted as individual indexed peaks and the amorphous halo. An example of such a deconvolution is also plotted in Figure 6 as discontinuous lines for the initially amorphous sample. As mentioned before for the applied strains in region I, the linear WAXS profile taken from the isotropic diffraction pattern remains unchanged. However, in region II, some of the distinct Bragg reflections begin to disappear, leaving only (010) and (100) reflections although they are also severely smeared. The corresponding SAXS patterns in region II also exhibit distinct changes when compared with the patterns in region I. In region II, the SAXS patterns do not show any isotropic component. Two elongated scattering lobules begin to appear along the meridian, together with a sharp scattering streak along the equator. The long spacing along the meridional intensity profile can be calculated from Figure 3 using eq 1. In Figure 4, the long spacing value is found to decrease rapidly in the beginning of region II, where it levels off to a value similar to that of the initial sample at the end of this region.

The mechanical behavior in region III is characterized by a leveling off in the stress values with increasing strain. In the corresponding WAXS patterns, the equatorial reflections (010) and (100) predominantly appear in the equator with almost no evidence of the initial isotropic Bragg reflections. The SAXS patterns in this region are very similar to those observed in region II, but they are located at higher scattering angles, indicating a lower value of long spacing. The position of the meridional scattering maximum remains constant with strain in this region, as is clearly shown by the long spacing response (Figure 4, region III). However, the scattering lobules become more elongated in region III when compared to those in region II.

Discussion

The above results indicate that the applied macroscopic strain induces considerable changes in the microscopic structures of the block copolymer system. Herein, we attempt to discuss the molecular mechanisms on the basis of the three regions identified earlier.

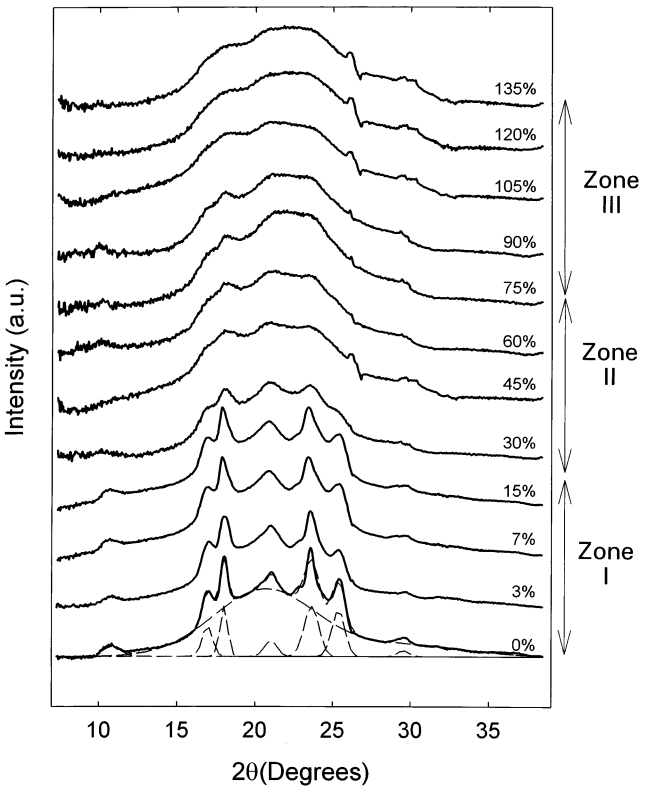

Figure 6. Integrated WAXS intensity profiles from the WAXS patterns during in-situ deformation. The labels indicate the applied strain in each case. Discontinuous lines show as an example the deconvolution procedure followed to obtain the width of the crystalline reflections.

Region I (0% < ϵ < 12%). The isotropic distributions of the SAXS/WAXS intensities obtained from the initial sample indicate a random orientation of the semicrystalline PBT domains in the sample. One observes a clear increase in the long spacing, together with the distortion of the SAXS patterns from the initial circular into an ellipsoidal shape having long axis aligned along the equator and the scattered intensity concentrated on the meridian. This indicates that the crystalline domains reoriented themselves as lamellar structure oriented perpendicular to the stretching direction. At the molecular level, both crystalline (PBT) and amorphous (PTMO) chains are aligned along the stretching direction. As the strain increases, the amorphous PTMO chains are elongated, but the crystalline PBT chains remain unchanged, resulting in an increase of the separation distance between the crystalline PBT domains. An earlier deformation study of initially stretched PBT−PTMO copolymers showed an affine relationship between the long spacing and the applied strain.[7] This is also nearly the same in our case. The slight deviation in the very initial stage is due to the rotation of the crystalline domains by the applied stress. The undisturbed WAXS patterns suggest that the applied strain is not sufficient to deform the crystalline structure in the PBT domains. Thus, the observed increase in stress is mainly due to the deformation of amorphous PTMO chains. In other words, the stress−strain relationship in this region are elastic and reversible because there is not permanent change in the hard segment domains. Upon relaxation, the deformation of the amorphous chains was found to be completely recovered, which has also been observed in a previous study for a similar polymer.[11]

Region II (12% < ϵ < 75%). After reaching the yield point (approximately at a strain of 12%), the rate of increase in stress becomes much smaller than that in region I (see Figure 2). No abrupt transition changes were observed in either SAXS or WAXS patterns. In this region, the SAXS pattern exhibits two discrete scattering peaks in the meridian and a diffuse scattering streak along the equator. These results are consistent with the lamellar structure changes in homopolymers (such as polyethylene and polypropylene), although the detailed mechanism is different. During plastic deformation in the neck region of homopolymers, the lamellae of folded chain crystals can be broken down into smaller pieces, which then can be reassembled into a microfibrillar structure along the stretching direction to minimize the local stress.[12,13] All the lamellae are aligned perpendicular to the draw direction, while the chains are parallel to that. This morphological evolution can also be applied to explain the observed SAXS/WAXS results in this study. The meridional SAXS maxima indicate the existence of layered lamellae that are aligned, on the average, perpendicular to the stretching direction. The equatorial SAXS streak reveals that the lamellae are beginning to assemble into a microfibrillar structure. The oriented WAXS patterns indicate that the crystalline PBT chains are aligned nearly parallel to the stretch direction. However, there is a distinct difference between the morphological changes of semicrystalline homopolymers and segmented copolymers with crystalline hard segment domains: there is no destruction of the crystalline lamellar structure in copolymers; the morphological changes are mainly due to the reorientation of the crystalline hard domains.

The feature of the strain-induced microfibrils can be further examined in the observed WAXS patterns. In WAXS, the appearance of spotlike equatorial reflections indicates a high degree of crystal orientation in the sample. The width of these equatorial reflections, however, is found to increase with increasing strain in region II (see Figure 6). It is well-known that the width of the reflections is an indication of the crystal perfection. The lower the crystal perfection is, the larger the reflection width becomes. From the integrated WAXS intensities, the apparent crystallite size (ACS) was calculated using the Scherrer equation:[14]

$$\mathrm{ACS} = \frac{0.9\lambda}{(\Delta 2\theta)\cos\theta} \tag{4}$$

where λ is the X-ray wavelength, ($\Delta 2\theta$) is the width at half-maximum of the crystalline peak in radians, and θ is half the value of the 2θ position of the center of the crystallite peak. In Figure 7, the ACS is presented as a function of applied strain. As before, the strain−stress curve is superimposed for the sake of comparison. In region III, this analysis was not possible due to the broadness of the reflections. The above results suggest that, upon the formation of microfibrils, the strain increase directly affects the perfection in crystals. In line with this, the elongation of the meridional SAXS reflections in the equatorial direction decreases with increasing stress, indicating that some crystalline lamellae oriented perpendicular to the stretching direction may be broken down, resulting in a decrease in long period which has been observed before.[15] The mechanism for this "destruction" will be discussed below. It needs to be pointed out that although the equatorial streak in SAXS has been frequently attributed to the formation of microvoids in the sample during stretching, a recent study in a similar polymer has associated this features to the so-called soft phase needles formed by the elongated soft segments.[16]

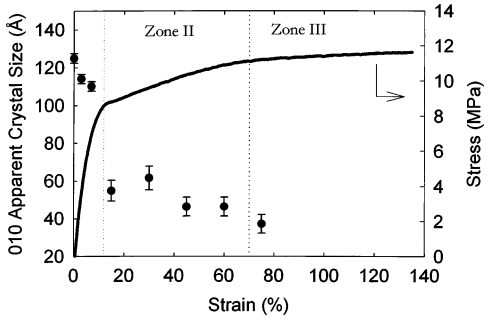

Figure 7. Apparent crystallite size (ACS) as a function of the applied strain (●). For comparison, the stress−strain curve is superimposed as a continuous line.

Region III (ϵ > 75%). In this region, the sample is fractured at high strains. This region is different from region II in two aspects. First, the rate of increase in stress is almost negligible. Second, the breadth of the meridional SAXS scattering peak (panels 6 and 7 in Figure 2) measured perpendicular to the stretching (equatorial direction) is broader than that in region II, and it does not change with increasing strain. This breadth of the meridional scattering peak along the equatorial direction is inversely proportional to the domain width (or the lamellar width in this case); i.e., the broader the peak is, the shorter the lamellae become. This fact is reflected in the meridional projected intensity $I_1(q_3)$ and in the obtained structural parameters from the correlation function analysis (Table 1). The values of L_c^{M1} and L_c^{m1} values are very different for all the cases. However, in region III, they are closer to each other, indicating that probably the width of the distribution of lamellar thickness decreases and the remaining crystallites are very small. The SAXS results are also consistent with the widths of equatorial WAXS reflections (see Figure 7). As one sees in Figure 5, the widths of the two dominant reflections become broader at the later stages of region II and do not change further with increasing strain. These results indicate that, in region III, the crystals have already been broken down into small pieces prior to fracture. In other words, the continuous "destruction" of the crystallites is mostly concentrated in region II after the yield point. In region III, no further change in the crystalline domain is observed. The SAXS equatorial streak is more prominent in this region. Assuming a model of rodlike fibrils, and using the Guinier analysis[17] of this equatorial streak, the lateral dimension R of the microfibrils can be estimated. The equatorial SAXS intensity at very low angles can be expressed as

$$I(q_{12}) \propto \exp\left(-\frac{{q_{12}}^2 R^2}{4}\right) \tag{5}$$

In this region before the fracture of the sample occurs, the obtained values for R are approximately 200 Å.

It is conceivable that as chain breakage occurs in a local region, the stress concentration around the broken chain can be increased significantly, eventually resulting in more breakages and the fracture of the sample.

Deformation-Induced Structure Changes from Samples of Different States. Several models have

been proposed to explain the structure changes during deformation of segmented copolymers with and without orientation.[7,8,11] As our system is quite similar to the one studied by Fakirov et al.[7] and by Stribeck,[16] we would like to examine our results in light of the model proposed by these authors. Fakirov et al. argued that, in predrawn poly(ether ester) copolymers, the reversible part of the structural changes was due to an affine deformation between the lamellae within the microfibrils. Above a critical strain, some of the microfibrils begin to lose connections with adjacent ones, and they can relax, giving rise to the appearance of a second long spacing similar to the one observed in the initial sample. In this study, however, the second long spacing was never observed, probably because the connections between the microfibrils were always tight, which is consistent with the observation of sample fracture at a relatively low strain. The main difference between the experiments by Fakirov et al.[7,16] and the present study was the state of the initial sample. In previous cases, the initial sample was highly oriented due to pretreatments including drawing to 5 times of the initial length and subsequent annealing at high temperatures and the applied strain. These pretreatments might have induced many microfibrils, uncorrelated with each other. In this study, however, the initial sample was isotropic. It is conceivable that drawing of the isotropic sample above the yield point might have induced highly interconnected microfibrils. Thus, we believe that the amount of tie molecules between the microfibrils in the sample drawn from the isotropic state is much higher than that in the predrawn and annealed samples. This argument is also consistent with the observations that the crystalline morphology in the current study was much more affected by the applied stress than that in the predrawn sample by Fakirov et al. This is quite reasonable as the morphology of the isotropic sample was without preferred orientation; the applied stress could cause substantial rotation and rearrangement of the lamellae in the initial stages of deformation. In contrast, the crystalline morphology in the predrawn sample was already well oriented, resulting in being less affected by subsequent deformation.

At this point, the possible effect of deformation on the crystal structure change should also be discussed. It is known that semicrystalline PBT suffers a change from the α to β crystalline form as stress is applied. Such a solid-state phase transition is due to the different conformations of the methylene segments in PBT under strain. In the chosen block copolymer system, the phase transition has also been observed by Tashiro et al.,[18] when the internal stress around the crystalline domain was sufficiently high. However, in this study, a direct identification of this effect was not possible because the positions of the (010) and (100) reflections in both crystal forms (α and β) are very similar.[19] The relatively poor crystalline perfection and the small crystal size in the isotropic sample have severely hindered us to examine the small shifts in the reflections due to the possible transformation of different crystal forms. However, a solid-state transformation is very likely to occur at strains just prior to the destruction of the crystalline domains, since the internal stress at that point should be very high.

Conclusions

1. The relationships between the macroscopic uniaxial stretching deformation and the changes of structure at both molecular and lamellar levels in a thermoplastic elastomer have been explored by means of simultaneous two-dimensional SAXS and WAXS. Three regions in the stress−strain curve were identified.

2. In region I (elastic response) the strain was found to induce the elongation of amorphous chains and the orientation of crystalline domains. As a result, the lamellae are aligned perpendicular to the drawing direction, and both amorphous PTMO chains and crystalline PBT chains are parallel to the stretching.

3. In region II, after surpassing the yield point, the strain was found to cause irreversible breakage of the PBT crystalline lamellae. At higher strains, the broken lamellae appeared to reassemble themselves along the stretching direction interconnected by tie molecules, forming microfibrils.

4. In region III, the increase in strain caused the amorphous PTMO chains to break.

5. The possibility of a strain induced solid-state phase transformation in the PBT crystals is likely to occur. However, such a transformation could not be positively identified in the present study.

Acknowledgment. Z. Denchev gratefully acknowledges the tenure of a fellowship awarded by the Spanish Ministry of Culture and Education (5B97-K5447945). A. Nogales thanks Dr. T. González-Lezana for his helpful discussions. The authors thank the financial support from the Full-Bright commission and the DGICYT (Grant PB 94-0049). B. Hsiao also acknowledges the financial support by NSF (DMR-0098104).

References and Notes

(1) Adams, R. K.; Hoeschele, G. K. Thermoplastic Polyester Elastomers. In *Thermoplastic Elastomers: A Comprenhensive Review*; Legge, N. R., Holden, G., Schroeder, H. E., Eds.; Hanser Publishers: New York, 1996.
(2) Baltá-Calleja, F. J.; Fakirov, S.; Roslaniec, Z.; Krumova, M.; Ezquerra, T. A.; Rueda, D. R. *J. Macromol Sci., Phys. B* **1998**, *37*, 219.
(3) Schroeder, H.; Cella, R. J. *Encyclopedia of Polymer Science and Engineering;* John Wiley & Sons: New York, 1988; Vol. 12.
(4) Wegner, G.; Fuji, T.; Meyer, W.; Liesser, G. *Angew. Makromol. Chem.* **1978**, *74*, 295.
(5) Tashiro, K.; Nakai, Y.; Kobayashi, M.; Tadokoro, H. *Macromolecules* **1980**, *13*, 137.
(6) Tashiro, K.; Hiramatsu, M.; Ti, T. *J. Soc. Fiber Technol., Jpn.* **1986**, *42*, T-597.
(7) Fakirov, S.; Fakirov, C.; Fischer, E. W.; Stamm, M. *Polymer* **1991**, *32*, 1173.
(8) Stribeck, N.; Sapoundjieva, D.; Denchev, Z.; Apostolov, A. A.; Zachmann, H. G.; Stamm, M.; Fakirov, S. *Macromolecules* **1997**, *30*, 1329.
(9) Mencik, Z. *J. Polym. Sci., Polym. Phys. Ed.* **1975**, *13*, 2173.
(10) Strobl, G. R.; Schneider, M. *J. Polym. Sci.* **1980**, *18*, 1343.
(11) Fakirov, S.; Fakirov, C.; Fischer, E.W.; Stamm, M.; Apostolov, A. A. *Colloid Polym. Sci.* **1993**, *271*, 811.
(12) Baltá-Calleja, F. J.; Peterlin, A. *J. Macromol. Sci., Phys. B* **1970**, *4*, 519.
(13) Baltá-Calleja, F. J.; Peterlin, A. *Kolloid Z.* **1972**, *242*, 1093.
(14) Guinier, A. *X-ray Diffraction in Crystals, Imperfect Crystals and Amorphous Bodies;* Freeman: San Francisco, 1963.
(15) Pakula, T.; Saijo, K.; Kawai, H.; Hashimoto, T. *Macromolecules* **1985**, *18*, 1294.
(16) Stribeck, N. *J. Polym. Sci., Part B: Polym. Phys.* **1999**, *37*, 975.
(17) Guinier, A.; Fournet, G. *Small Angle Scattering of X-rays;* Wiley: New York, 1955.
(18) Tashiro, K.; Hiramatsu, M.; Ti, T. *J. Soc. Fiber Technol., Jpn.* **1986**, *42*, T-659.
(19) Yokouchi, M.; Sakakibara, Y.; Chatani, Y.; Tadokoro, H.; Tanaka, T.; Yoda, K. *Macromolecules* **1976**, *9*, 266.

MA0210877